IJMMM
International Journal of
Minerals, Metallurgy and Materials
矿物冶金与材料学报（英文版）

Thermodynamic model for deoxidation of liquid steel considering strong metal–oxygen interaction in the quasichemical model framework

Yong-Min Cho and Youn-Bae Kang

Cite this article as:
Yong-Min Cho and Youn-Bae Kang, Thermodynamic model for deoxidation of liquid steel considering strong metal–oxygen interaction in the quasichemical model framework, *Int. J. Miner. Metall. Mater.*, 31(2024), No. 5, pp. 988-1002. https://doi.org/10.1007/s12613-023-2766-7

View the article online at SpringerLink or IJMMM Webpage.

Articles you may be interested in

Uttam Bhandari, Congyan Zhang, Shengmin Guo, and Shizhong Yang, First-principles study on the mechanical and thermodynamic properties of MoNbTaTiW, *Int. J. Miner. Metall. Mater.*, 27(2020), No. 10, pp. 1398-1404. https://doi.org/10.1007/s12613-020-2077-1

Tian Qiu, Jian-guo Yang, and Xue-jie Bai, Insight into the change in carbon structure and thermodynamics during anthracite transformation into graphite, *Int. J. Miner. Metall. Mater.*, 27(2020), No. 2, pp. 162-172. https://doi.org/10.1007/s12613-019-1859-9

Chao-qun Cui, Bing Wang, Yi-xin Zhao, Yong-Jin Zhang, and Li-ming Xue, Risk management for mine closure: A cloud model and hybrid semi-quantitative decision method, *Int. J. Miner. Metall. Mater.*, 27(2020), No. 8, pp. 1021-1035. https://doi.org/10.1007/s12613-020-2002-7

Fei Yuan, An-jun Xu, and Mao-qiang Gu, Development of an improved CBR model for predicting steel temperature in ladle furnace refining, *Int. J. Miner. Metall. Mater.*, 28(2021), No. 8, pp. 1321-1331. https://doi.org/10.1007/s12613-020-2234-6

Wei Xiao, Yan-ping Bao, Chao Gu, Min Wang, Yu Liu, Yong-sheng Huang, and Guang-tao Sun, Ultrahigh cycle fatigue fracture mechanism of high-quality bearing steel obtained through different deoxidation methods, *Int. J. Miner. Metall. Mater.*, 28(2021), No. 5, pp. 804-815. https://doi.org/10.1007/s12613-021-2253-y

Sajjad Ali, Yaseen Iqbal, Inamullah Khan, Ansar Ullah, Muhammad Sadiq, Muhammad Fahad, and Khizar Hussain Shah, Hydrometallurgical leaching and kinetic modeling of low-grade manganese ore with banana peel in sulfuric acid, *Int. J. Miner. Metall. Mater.*, 28(2021), No. 2, pp. 193-200. https://doi.org/10.1007/s12613-020-2069-1

IJMMM WeChat

QQ author group

INTERNATIONAL JOURNAL OF
Minerals, Metallurgy and Materials

Volume 31, Number 5, May 2024
Page 988

Research Article https://doi.org/10.1007/s12613-023-2766-7

Thermodynamic model for deoxidation of liquid steel considering strong metal–oxygen interaction in the quasichemical model framework

Yong-Min Cho[1,2] *and Youn-Bae Kang*[1,3),✉]

1) Graduate Institute of Ferrous and Eco Materials Technology, Pohang University of Science and Technology, Pohang, Kyungbuk, 37673, Rep. of Korea
2) N.EX.T Hub, POSCO Holdings, Pohang, Kyungbuk, 37673, Rep. of Korea
3) Department of Materials Science and Engineering, Pohang University of Science and Technology, Pohang, Kyungbuk, 37673, Rep. of Korea

(Received: 18 July 2023; revised: 13 October 2023; accepted: 20 October 2023)

Abstract: Herein, a thermodynamic model aimed at describing deoxidation equilibria in liquid steel was developed. The model provides explicit forms of the activity coefficient of solutes in liquid steel, eliminating the need for the minimization of internal Gibbs energy preliminarily when solving deoxidation equilibria. The elimination of internal Gibbs energy minimization is particularly advantageous during the coupling of deoxidation equilibrium calculations with computationally intensive approaches, such as computational fluid dynamics. The model enables efficient calculations through direct embedment of the explicit forms of activity coefficient in the computing code. The proposed thermodynamic model was developed using a quasichemical approach with two key approximations: random mixing of metallic elements (Fe and oxidizing metal) and strong nonrandom pairing of metal and oxygen as nearest neighbors. Through these approximations, the quasichemical approach yielded the activity coefficients of solutes as explicit functions of composition and temperature without requiring the minimization of internal Gibbs energy or the coupling of separate programs. The model was successfully applied in the calculation of deoxidation equilibria of various elements (Al, B, C, Ca, Ce, Cr, La, Mg, Mn, Nb, Si, Ti, V, and Zr). The limitations of the model arising from these assumptions were also discussed.

Keywords: deoxidation equilibria; thermodynamics; quasichemical approach; computational fluid dynamics

1. Introduction

The quality of liquid steel during secondary refining plays an important role in the quality control of steel products. Deoxidation, as one of the refining reactions, plays a crucial role in determining the quality of liquid steel. This process affects important factors, such as cleanliness in relation to non-metallic inclusion evolution [1] and blow hole formation [2]. Numerous approaches have been developed to predict deoxidation equilibria in liquid steel [3–11]. When coupled with computational fluid dynamics (CFD) calculations, deoxidation equilibrium calculations enable the simulation of composition evolution in the liquid steel within vessels (ladle, tundish, and mold). As a result, spatial and temporal distributions of the composition of the liquid steel as well as those of the non-metallic inclusions can be analyzed. This capability can assist steel plant operators in assessing the control of liquid-steel composition.

The reliability of a thermodynamic model determines the accuracy of deoxidation equilibrium calculations. Wagner's interaction parameter formalism (WIPF) is popularly used in this context [12]. WIPF can be used to determine the solute activity coefficients of liquid steel as explicit functions of composition and temperature. According to this formalism, the activity coefficient of solute i can be expressed as follows [12–14]:

$$\lg f_{\underline{i}} = e_i^j[\%j] + e_i^k[\%k] + \cdots + r_i^j[\%j]^2 + r_i^k[\%k]^2 + \cdots \quad (1)$$

on the mass percentage base or

$$\ln \gamma_{\underline{i}} = \varepsilon_i^j X_j + \varepsilon_i^k X_k + \cdots + \rho_i^j X_j^2 + \rho_i^k X_k^2 + \cdots \quad (2)$$

on the mole fraction base, where e_i^j, r_i^j, ε_i^j, and ρ_i^j are the first- and second-order interaction parameters on the mass percentage base between i and j, and those on the mole fraction base, resepctively [13–14]. These equations, which are collectively called formalism, provide activity coefficients as explicit functions of composition and temperature. However, this formalism does not originate from a comprehensive thermodynamic model and has certain limitations [7,15–18]. Notably, it lacks full thermodynamic consistency [15–17,19] and may be inapplicable to systems with highly remarkable interactions. Nonetheless, this type of formalism has gained popularity due to its simplicity. Additional calculations are unnecessary in determining the activity coefficient, easing the direct implementation of WIPF in computational codes such as CFD. Therefore, Eqs. (1) or (2) can be directly utilized in CFD or other computing codes to conduct thermodynamic calculations.

Alternatively, modern CALPHAD software tools, such as

✉ Corresponding author: Youn-Bae Kang E-mail: ybkang@postech.ac.kr
© University of Science and Technology Beijing 2024
Springer

FactSage [20–21] and ThermoCalc [22], can be used to solve deoxidation equilibria using the available appropriate thermodynamic models and databases. These software packages also provide application programming interfaces (APIs), such as ChemApp [23] and TC-Python [22], which allow users to develop their own customized application programs. One possible application is the coupling of CALPHAD-API with CFD codes, in which iterative calculations between the two are performed. However, not only the accuracy and reliability of the selected thermodynamic model but also the computation cost associated with the required calculation steps must be considered when developing a user-specific application program. Successive iterations between CALPHAD-API and CFD code can considerably increase the computation time.

The present authors are currently developing a tundish process simulator that can accurately calculate the composition evolution of Al-killed liquid steel, with a unique focus on the concentration profiles of Al, O, and alumina inclusions in liquid steel, under time and space scales [24]. The extensive computational cost involved implies the need for the minimization of computation steps while ensuring reliability. One potential approach is deoxidation equilibrium calculations within the CFD code itself, which eliminates the need for external CALPHAD-API software and reduces the cross-calling time between two software components. However, as highlighted by Kang [18], sophisticated thermodynamic models are required in the accurate prediction of deoxidation equilibria. The modified quasichemical model (MQM) in the pair approximation, employed by FactSage software, has shown great promise in describing deoxidation equilibria in liquid steel; it has been successfully used in the treatment of deoxidation by Al and Mn [11,25]. These advanced thermodynamic models typically involve an additional step known as internal Gibbs energy minimization. Consequently, the Gibbs energy of the liquid phase cannot be expressed simply as a function of composition and temperature. An internal minimization routine involving Gibbs energy must be used to obtain the Gibbs energy for a given composition and temperature. As a result, the activity coefficients of solutes cannot be explicitly expressed as functions of composition and temperature but were rather obtained implicitly after the internal equilibrium is solved. This limitation restricts the direct incorporation of such thermodynamic models into the CFD code. Therefore, a thermodynamic model for deoxidation equilibria that does not require internal Gibbs energy minimization should be developed while maintaining a high level of accuracy.

The present study introduces a thermodynamic model that does not require the internal Gibbs energy minimization for deoxidation equilibria of liquid steel. The model demonstrates accuracy and reliability across a wide range of compositions and temperatures for deoxidation equilibria involving various elements in liquid steel. Furthermore, the model successfully handles complex deoxidation equilibria involving elements such as Al and Mn. Lastly, the present study presents an example showcasing the coupling of the proposed model with a CFD code to predict the composition profile of liquid steel in a tundish process.

2. Thermodynamic approaches for deoxidation equilibria of liquid steel

2.1. Deoxidation equilibria

A well-known deoxidation reaction in liquid steel occurs due to the presence of Al:

$$2\underline{\mathrm{Al}}+3\underline{\mathrm{O}}=\mathrm{Al_2O_3(s)},\ \Delta G^{\ominus,\prime}_{\mathrm{Al_2O_3}}=-RT\ln K'_{\mathrm{Al_2O_3}} \tag{3}$$

where $\Delta G^{\ominus,\prime}_{\mathrm{Al_2O_3}}$ is the standard Gibbs energy change of reaction (3). The equilibrium constant of this reaction is as follows:

$$K'_{\mathrm{Al_2O_3}}=\frac{a_{\mathrm{Al_2O_3(s)}}}{a^2_{\underline{\mathrm{Al}}}a^3_{\underline{\mathrm{O}}}} \tag{4}$$

When the reaction product is pure, e.g., $a_{\mathrm{Al_2O_3(s)}}=1$, then the equilibrium constant $K'_{\mathrm{Al_2O_3(s)}}$ is calculated using the following equation:

$$K'_{\mathrm{Al_2O_3}}=\frac{1}{\left(\gamma_{\underline{\mathrm{Al}}}X_{\mathrm{Al}}\right)^2\left(\gamma_{\underline{\mathrm{O}}}X_{\mathrm{O}}\right)^3} \tag{5}$$

When the values of $\gamma_{\underline{\mathrm{Al}}}$ and $\gamma_{\underline{\mathrm{O}}}$ (relative to the infinite dilution standard state or Henrian standard state) are known, they can be substituted into Eq. (5). The equation is then solved to establish the relationship between X_{Al} and X_{O} at equilibrium.

In general, a metal element ($\underline{\mathrm{M}}$) reacts with dissolved $\underline{\mathrm{O}}$ via the following:

$$x\underline{\mathrm{M}}+y\underline{\mathrm{O}}=\mathrm{M}_x\mathrm{O}_y,\ \Delta G^{\ominus,\prime}_{\mathrm{M}_x\mathrm{O}_y}=-RT\ln K'_{\mathrm{M}_x\mathrm{O}_y} \tag{6}$$

where $\Delta G^{\ominus,\prime}_{\mathrm{M}_x\mathrm{O}_y}$ is the standard Gibbs energy change of reaction (6), and

$$K'_{\mathrm{M}_x\mathrm{O}_y}=\frac{1}{\left(\gamma_{\underline{\mathrm{M}}}X_{\mathrm{M}}\right)^x\left(\gamma_{\underline{\mathrm{O}}}X_{\mathrm{O}}\right)^y} \tag{7}$$

where

$$\Delta G^{\ominus,\prime}_{\mathrm{M}_x\mathrm{O}_y}=G^{\ominus}_{\mathrm{M}_x\mathrm{O}_y}-xG^{\ominus}_{\underline{\mathrm{M}}}-yG^{\ominus}_{\underline{\mathrm{O}}} \tag{8}$$

The Raoultian standard state can be used as an alternative to the infinite dilution standard state:

$$x\mathrm{M}+y\mathrm{O}=\mathrm{M}_x\mathrm{O}_y,\ \Delta G^{\ominus}_{\mathrm{M}_x\mathrm{O}_y}=-RT\ln K_{\mathrm{M}_x\mathrm{O}_y} \tag{9}$$

$$K_{\mathrm{M}_x\mathrm{O}_y}=\frac{1}{(\gamma_{\mathrm{M}}X_{\mathrm{M}})^x(\gamma_{\mathrm{O}}X_{\mathrm{O}})^y} \tag{10}$$

where

$$\Delta G^{\ominus}_{\mathrm{M}_x\mathrm{O}_y}=G^{\ominus}_{\mathrm{M}_x\mathrm{O}_y}-xG^{\ominus}_{\mathrm{M}}-yG^{\ominus}_{\mathrm{O}} \tag{11}$$

where $G^{\ominus}_i$ refers to the molar Gibbs energies of pure i.

The relation between $G^{\ominus}_i$ and $G^{\ominus}_{\underline{i}}$ is as follows:

$$G^{\ominus}_i=G^{\ominus}_{\underline{i}}+RT\ln\gamma^{\ominus}_i \tag{12}$$

where $\gamma^{\ominus}_i$ represents the activity coefficient at the infinite dilution of i.

2.2. Explicit expression of activity coefficient as a function of composition

$\gamma_{\underline{\mathrm{M}}}$ and $\gamma_{\underline{\mathrm{O}}}$ are typically functions of composition (X_k, $k=$

M or O) and temperature (T). According to WIPF [12,14], these functions can be expressed as follows:

$$\ln \gamma_{\underline{\mathrm{M}}} = \varepsilon_{\mathrm{M}}^{\mathrm{M}} X_{\mathrm{M}} + \varepsilon_{\mathrm{M}}^{\mathrm{O}} X_{\mathrm{O}} + \cdots \tag{13}$$

$$\ln \gamma_{\underline{\mathrm{O}}} = \varepsilon_{\mathrm{O}}^{\mathrm{O}} X_{\mathrm{O}} + \varepsilon_{\mathrm{O}}^{\mathrm{M}} X_{\mathrm{M}} + \cdots \tag{14}$$

where ε_i^js are the first-order interaction parameters among solutes. $K_{\mathrm{M}_x\mathrm{O}_y}$ and ε_i^js can be obtained from literature [14,26]. Substitution of these parameters into Eq. (5) along with Eqs. (13) and (14) can be used to determine the equilibrium composition of liquid steel. Examples of methods belonging to this category include the Unified Interaction Parameter Formalism and Darken's quadratic formalism [15,17,27–28].

Activity coefficients can also be derived from the excess Gibbs energy of mixing of the liquid solution:

$$RT\ln \gamma_i = \left.\frac{\partial G^{\mathrm{ex}}}{\partial n_i}\right|_{n_j \neq n_i} \tag{15}$$

where total excess Gibbs energy (G^{ex} in J) can be expressed as an explicit function of T and the number of moles of components (e.g., n_i). This relationship holds in cases involving a regular solution model or a random mixing model with polynomial expansions for excess Gibbs energy [8,17].

Notably, Eq. (5) does not provide the explicit form of composition (X_k), which indicates the need for a numerical approach to obtain a deoxidation equilibrium data point. The results can be readily expressed as mass percent ([%M]). Fig. 1 provides an overview of this approach.

2.3. Implicit expression for the activity coefficient

When G^{ex} is not an explicit function of composition, the activity coefficient obtained from Eq. (15) also lacks explicit dependence on composition. This situation often occurs during the deviation of a solution from random mixing behavior, such as in the case of an associate solution model featuring a strong chemical attraction (short-range ordering, SRO) [3,7,29]. Bouchard and Bale [29] reported the successful application of this model in the deoxidation equilibria of liquid steel; in this case, in addition to unassociated Al and O, Al*O and $\mathrm{Al_2}$*O associates were assumed to be present in Al-deoxidized liquid steel. Jung *et al.* [7] further extended this approach to other systems and effectively described the deoxidation equilibria of M in liquid steel up to high M concentrations. However, these approaches require internal Gibbs energy minimization to determine the number of associates before the activity coefficient can be calculated, which adds an additional step to calculations. Other thermodynamic approaches requiring internal Gibbs energy minimization to address SRO, such as the MQM [30–31] and Generalized Central Atoms model [32], are applied in the same context.

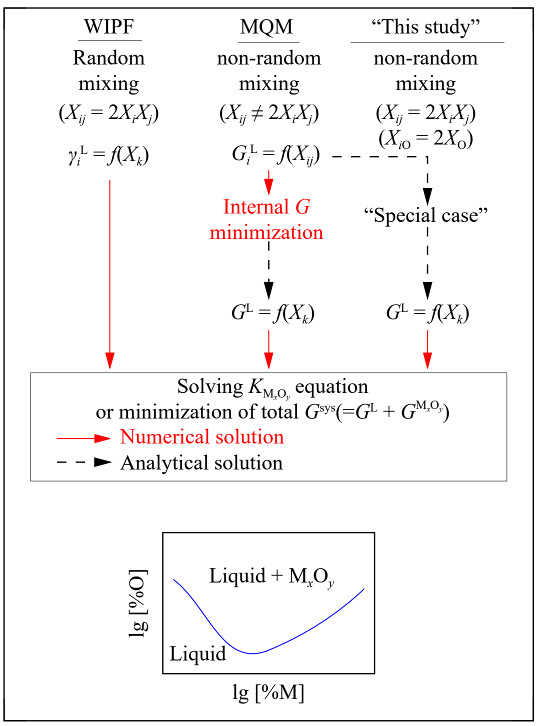

Fig. 1. Overview of deoxidation equilibrium–calculation approaches.

In the present study, a novel model was presented to handle the deoxidation of liquid steel without internal Gibbs energy minimization. The model considers strong SRO under limiting conditions to eliminate the requirement for internal Gibbs energy minimization. In addition, the model is based on a simplified quasichemical model, which will be discussed in Section 4.

3. MQM in the pair approximation for deoxidation equilibria

Pelton *et al.* proposed a modification of the classical quasichemical approach [33], known as the MQM in the pair [30] and the quadruplet approximations [31]. This model has been successfully applied in various solution systems, including liquid metals [34–36] and liquid oxides [37–40] using MQM in the pair approximation and liquid oxysulfides [41–42] and liquid oxyfluorides [43] using MQM in the quadruplet approximation. Specifically, MQM in the pair approximation has been successfully applied to model deoxidation equilibria in liquid steel involving elements such as Al [11], Mn [25], and Al–Mn [25].

In the deoxidation of liquid steel by M (Fe–M–O liquid solution), the following pair-exchange reactions are considered:

$$(\mathrm{Fe-Fe}) + (\mathrm{M-M}) = 2(\mathrm{Fe-M}),\ \Delta g_{\mathrm{FeM}} \tag{16}$$

$$(\mathrm{Fe-Fe}) + (\mathrm{O-O}) = 2(\mathrm{Fe-O}),\ \Delta g_{\mathrm{FeO}} \tag{17}$$

$$(\mathrm{M-M}) + (\mathrm{O-O}) = 2(\mathrm{M-O}),\ \Delta g_{\mathrm{MO}} \tag{18}$$

where $(i-j)$ and Δg_{ij} (which is usually a function of composition and temperature) refer to the first-nearest-neighbor (FNN) pair $i-j$ and pair formation energy, respectively.

The number of moles of each pair (n_{ij}) is related to the number of moles of each component (n_i) through the FNN coordination numbers (Z_i):

$$Z_{\mathrm{Fe}} n_{\mathrm{Fe}} = 2n_{\mathrm{FeFe}} + n_{\mathrm{FeM}} + n_{\mathrm{FeO}} \tag{19}$$

$$Z_{\mathrm{M}}n_{\mathrm{M}} = 2n_{\mathrm{MM}} + n_{\mathrm{FeM}} + n_{\mathrm{MO}} \tag{20}$$

$$Z_{\mathrm{O}}n_{\mathrm{O}} = 2n_{\mathrm{OO}} + n_{\mathrm{FeO}} + n_{\mathrm{MO}} \tag{21}$$

The Gibbs energy of the liquid solution is then expressed as follows [30]:

$$G^{\mathrm{L}} = n_{\mathrm{Fe}}g_{\mathrm{Fe}}^{\ominus} + n_{\mathrm{M}}g_{\mathrm{M}}^{\ominus} + n_{\mathrm{O}}g_{\mathrm{O}}^{\ominus} + RT\left(n_{\mathrm{Fe}}\ln X_{\mathrm{Fe}} + n_{\mathrm{M}}\ln X_{\mathrm{M}} + n_{\mathrm{O}}\ln X_{\mathrm{O}}\right) + G^{\mathrm{ex}} \tag{22}$$

where $g_i^{\ominus}$ is the molar Gibbs energy of pure liquid i, and

$$G^{\mathrm{ex}} = RT\left[n_{\mathrm{FeFe}}\ln\left(\frac{X_{\mathrm{FeFe}}}{Y_{\mathrm{Fe}}^2}\right) + n_{\mathrm{MM}}\ln\left(\frac{X_{\mathrm{MM}}}{Y_{\mathrm{M}}^2}\right) + n_{\mathrm{OO}}\ln\left(\frac{X_{\mathrm{OO}}}{Y_{\mathrm{O}}^2}\right) + n_{\mathrm{FeM}}\ln\left(\frac{X_{\mathrm{FeM}}}{2Y_{\mathrm{Fe}}Y_{\mathrm{M}}}\right) + n_{\mathrm{FeO}}\ln\left(\frac{X_{\mathrm{FeO}}}{2Y_{\mathrm{Fe}}Y_{\mathrm{O}}}\right) + n_{\mathrm{MO}}\ln\left(\frac{X_{\mathrm{MO}}}{2Y_{\mathrm{M}}Y_{\mathrm{O}}}\right)\right] + \frac{n_{\mathrm{FeM}}}{2}\Delta g_{\mathrm{FeM}} + \frac{n_{\mathrm{FeO}}}{2}\Delta g_{\mathrm{FeO}} + \frac{n_{\mathrm{MO}}}{2}\Delta g_{\mathrm{MO}} \tag{23}$$

where X_{ij} and Y_i indicate the pair fraction of $i-j$ pair and the coordinate equivalent fraction of i, respectively:

$$X_{ij} = \frac{n_{ij}}{n_{\mathrm{FeFe}} + n_{\mathrm{MM}} + n_{\mathrm{OO}} + n_{\mathrm{FeM}} + n_{\mathrm{FeO}} + n_{\mathrm{MO}}} \tag{24}$$

$$Y_i = \frac{Z_i n_i}{Z_{\mathrm{Fe}}n_{\mathrm{Fe}} + Z_{\mathrm{M}}n_{\mathrm{M}} + Z_{\mathrm{O}}n_{\mathrm{O}}} \tag{25}$$

Further details regarding the development of the model can be found elsewhere [30].

Given that Eq. (23) is not an explicit function of composition (e.g., X_{M}, X_{O}), differentiation through internal Gibbs energy minimization is required to obtain internal equilibrium:

$$\left.\frac{\partial G^{\mathrm{ex}}}{\partial n_{\mathrm{FeM}}}\right|_{n_{\mathrm{Fe}},n_{\mathrm{M}},n_{\mathrm{O}}} = \left.\frac{\partial G^{\mathrm{ex}}}{\partial n_{\mathrm{FeO}}}\right|_{n_{\mathrm{Fe}},n_{\mathrm{M}},n_{\mathrm{O}}} = \left.\frac{\partial G^{\mathrm{ex}}}{\partial n_{\mathrm{MO}}}\right|_{n_{\mathrm{Fe}},n_{\mathrm{M}},n_{\mathrm{O}}} = 0 \tag{26}$$

This process yields three equilibrium constants for quasi-chemical reactions (16)–(18):

$$\frac{X_{\mathrm{FeM}}^2}{X_{\mathrm{FeFe}}X_{\mathrm{MM}}} = 4\exp\left(-\frac{\Delta g_{\mathrm{FeM}}}{RT}\right) \tag{27}$$

$$\frac{X_{\mathrm{FeO}}^2}{X_{\mathrm{FeFe}}X_{\mathrm{OO}}} = 4\exp\left(-\frac{\Delta g_{\mathrm{FeO}}}{RT}\right) \tag{28}$$

$$\frac{X_{\mathrm{MO}}^2}{X_{\mathrm{MM}}X_{\mathrm{OO}}} = 4\exp\left(-\frac{\Delta g_{\mathrm{MO}}}{RT}\right) \tag{29}$$

For a given set of n_{Fe}, n_{M}, and n_{O}, six unknowns (n_{FeFe}, n_{MM}, n_{OO}, n_{FeO}, n_{MO}, and n_{FeM}) and six equations (Eqs. (26)–(29)) are involved. These equations are solved using numerical methods to obtain the values of n_{ij} at internal equilibrium. The obtained values can be back-substituted into Eq. (23) using Eqs. (19)–(21) to calculate G^{L}. Substitution of Eq. (23) into Eq. (15) yields the activity coefficients of M (γ_{M}) and O (γ_{O}).

4. Model development in the present study

This section proposes a new model for the deoxidation of liquid steel based on the MQM in pair approximation.

4.1. Assumptions

Among the six FNN pairs in the Fe–M–O liquid solution, (Fe–Fe), (M–M), and (Fe–M) are pairs between metallic elements, (Fe–O) and (M–O) are pairs between a metal and O, and (O–O) is a pair between two O atoms. The following assumptions were considered:

(1) To simplify the model, it was assumed the coordination numbers of all components in the Fe–M–O liquid solution are equal:

$$Z_{\mathrm{Fe}} = Z_{\mathrm{M}} = Z_{\mathrm{O}} = Z \tag{30}$$

Eq. (25) is reduced to the following:

$$Y_i = X_i \tag{31}$$

From Eqs. (19) to (21), the total number of moles of all FNN pairs is computed as follows:

$$n_{\mathrm{FeFe}} + n_{\mathrm{MM}} + n_{\mathrm{OO}} + n_{\mathrm{FeO}} + n_{\mathrm{MO}} + n_{\mathrm{FeM}} = \frac{Z}{2}\left(n_{\mathrm{Fe}} + n_{\mathrm{M}} + n_{\mathrm{O}}\right) = \frac{Z}{2}n \tag{32}$$

where $n = n_{\mathrm{Fe}} + n_{\mathrm{M}} + n_{\mathrm{O}}$.

The excess Gibbs energy is then expressed as follows:

$$G^{\mathrm{ex}} = RT\left(\frac{Z}{2}n\right)\left[X_{\mathrm{FeFe}}\ln\left(\frac{X_{\mathrm{FeFe}}}{X_{\mathrm{Fe}}^2}\right) + X_{\mathrm{MM}}\ln\left(\frac{X_{\mathrm{MM}}}{X_{\mathrm{M}}^2}\right) + X_{\mathrm{OO}}\ln\left(\frac{X_{\mathrm{OO}}}{X_{\mathrm{O}}^2}\right) + X_{\mathrm{FeM}}\ln\left(\frac{X_{\mathrm{FeM}}}{2X_{\mathrm{Fe}}X_{\mathrm{M}}}\right) + X_{\mathrm{FeO}}\ln\left(\frac{X_{\mathrm{FeO}}}{2X_{\mathrm{Fe}}X_{\mathrm{O}}}\right) + X_{\mathrm{MO}}\ln\left(\frac{X_{\mathrm{MO}}}{2X_{\mathrm{M}}X_{\mathrm{O}}}\right)\right] + \left(\frac{Z}{2}n\right)\left(\frac{X_{\mathrm{FeM}}}{2}\Delta g_{\mathrm{FeM}} + \frac{X_{\mathrm{FeO}}}{2}\Delta g_{\mathrm{FeO}} + \frac{X_{\mathrm{MO}}}{2}\Delta g_{\mathrm{MO}}\right) \tag{33}$$

(2) If Fe, M, and O mix randomly, then the probabilities of finding an $i-i$ pair and an $i-j$ pair ($i \neq j$) are X_i^2 and $2X_iX_j$, respectively. However, given the presence of strong SRO between metals (Fe and M) and O [18], $X_{\mathrm{FeO}} > 2X_{\mathrm{Fe}}X_{\mathrm{O}}$ and $X_{\mathrm{MO}} > 2X_{\mathrm{M}}X_{\mathrm{O}}$. In the presence of a highly pronounced SRO between metals and O, almost all O in the liquid steel forms Fe–O and M–O pairs, and the O–O pair becomes scarce. Fig. 2 illustrates a limiting case of the M–O binary solution, where all O atoms in the solution form M–O pairs. Whenever an O atom enters the liquid, a new M–O pair forms, which leads to the consumption of M–M pairs. Therefore, in the M–O binary solution, the following can be obtained:

$$X_{\mathrm{MO}} = 2X_{\mathrm{O}},\ X_{\mathrm{MM}} = 1 - 2X_{\mathrm{O}},\ X_{\mathrm{OO}} = 0 \tag{34}$$

Notably, this assumption is meaningful only when X_{O} is low.

Similar to the SRO observed between M and O, a strong SRO was assumed between Fe and O in the Fe–M–O ternary solution. However, random mixing of Fe and M was also assumed. As a result, the following approximations can be made in the dilute region of O:

$$X_{\mathrm{FeO}} + X_{\mathrm{MO}} = 2X_{\mathrm{O}} \tag{35}$$

$$X_{\mathrm{FeFe}} + X_{\mathrm{MM}} + X_{\mathrm{FeM}} = 1 - 2X_{\mathrm{O}} \tag{36}$$

$$X_{\mathrm{OO}} = 0 \tag{37}$$

Eqs. (35)–(37) are an extension of Eq. (34) to the ternary solution.

4.2. Model formulae

With the assumption of random mixing of metallic ele-

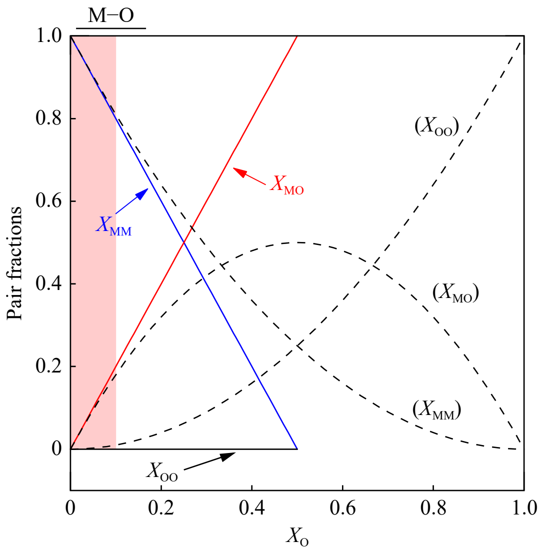

Fig. 2. Pair fraction X_{ij} in M–O binary liquid solution. Dashed lines represent the (X_{ij})s in the random mixing solution: $(X_{MM}) = X_M^2 = (1 - X_O)^2$, $(X_{OO}) = X_O^2$, and $(X_{MO}) = 2X_MX_O = 2(1 - X_O)X_O$. Solid lines indicate those in the strongly ordered solution. The present model can be defined up to $X_O = 0.5$ but is meaningful in the dilute region of O.

ments, the following equations can be derived:

$$X_{FeFe} = (1-2X_O)\times\left(\frac{X_{Fe}}{X_{Fe}+X_M}\right)^2 \tag{38}$$

$$X_{FeM} = (1-2X_O)\times\frac{2X_{Fe}X_M}{(X_{Fe}+X_M)^2} \tag{39}$$

$$X_{MM} = (1-2X_O)\times\left(\frac{X_M}{X_{Fe}+X_M}\right)^2 \tag{40}$$

At equilibrium, rearranging Eqs. (28) and (29) yields the following:

$$\frac{X_{MO}^2X_{FeFe}}{X_{FeO}^2X_{MM}} = \exp\left(-\frac{\Delta g_{MO}-\Delta g_{FeO}}{RT}\right) \equiv K_{MO}^2 \tag{41}$$

Substituting Eqs. (38) and (40) into Eq. (41) gives

$$\frac{X_{MO}}{X_{FeO}} = \frac{X_M}{X_{Fe}}K_{MO} \tag{42}$$

The relationship described above bears similarities to that proposed by Alcock and Richardson in their quasichemical approach [44]. However, the detailed development of their model differs from that used in the present study.

Along with Eq. (35), the above equation gives the following:

$$X_{FeO} = 2X_O\frac{X_{Fe}}{X_{Fe}+K_{MO}X_M} \equiv 2X_O\frac{X_{Fe}}{Q} \tag{43}$$

$$X_{MO} = 2X_O\frac{K_{MO}X_M}{X_{Fe}+K_{MO}X_M} \equiv 2X_O\frac{K_{MO}X_M}{Q} \tag{44}$$

where $Q \equiv X_{Fe} + K_{MO}X_M$. Therefore, with Eq. (31), the following equations are obtained:

$$\frac{X_{FeFe}}{Y_{Fe}^2} = \frac{X_{MM}}{Y_M^2} = \frac{X_{FeM}}{2Y_{Fe}Y_M} = \frac{1-2X_O}{(X_{Fe}+X_M)^2} \tag{45}$$

$$\frac{X_{FeO}}{2Y_{Fe}Y_O} = \frac{1}{Q} \tag{46}$$

$$\frac{X_{MO}}{2Y_MY_O} = \frac{K_{MO}}{Q} \tag{47}$$

Substitution of the above relationships, along with all X_{ij}s (Eqs. (38)–(40), (43), and (44)) yields the following:

$$G^{ex} = RT\left(\frac{Z}{2}n\right)\left[(1-2X_O)\ln\frac{1-2X_O}{(X_{Fe}+X_M)^2}+\frac{2X_O}{Q}\left(X_{Fe}\ln\frac{1}{Q}+K_{MO}X_M\ln\frac{K_{MO}}{Q}\right)\right]+\left(\frac{Z}{2}n\right)\left[\frac{X_O}{Q}(X_{Fe}\Delta g_{FeO}+K_{MO}X_M\Delta g_{MO})+\frac{X_{Fe}X_M}{(X_{Fe}+X_M)^2}(1-2X_O)\Delta g_{FeM}\right] \tag{48}$$

Through the substitution of Eq. (48) into Eq. (22), the complete expression of the Gibbs energy of the Fe–M–O ternary liquid solution can be obtained in the limiting case, which features an extreme SRO between the metal and oxygen (O), and random mixing exists between metallic elements.

4.3. Deoxidation equilibrium calculation

The activity coefficients of M and O (γ_M and γ_O) are obtained using Eq. (15):

$$\ln\gamma_M = \frac{Z}{2}\left[\ln\frac{1-2X_O}{(X_{Fe}+X_M)^2}+\frac{2X_O^2}{X_{Fe}+X_M}+\frac{2X_O(X_{Fe}+K_{MO}X_M-K_{MO})}{Q}+\frac{2K_{MO}X_{Fe}X_O}{Q^2}\ln K_{MO}\right]+\frac{Z}{2RT}\left[\frac{K_{MO}X_{Fe}X_O}{Q^2}(\Delta g_{MO}-\Delta g_{FeO})+\frac{X_{Fe}^2(X_{Fe}+X_M)-X_{Fe}X_O(X_{Fe}-X_M)}{(X_{Fe}+X_M)^3}\Delta g_{FeM}\right] \tag{49}$$

$$\ln\gamma_O = \frac{Z}{2}\left[\ln\frac{(X_{Fe}+X_M)^2}{1-2X_O}+\frac{2}{Q}\left(X_{Fe}\ln\frac{1}{X_{Fe}+K_{MO}X_M}+K_{MO}X_M\ln\frac{K_{MO}}{X_{Fe}+K_{MO}X_M}\right)\right]+\frac{Z}{2RT}\left[\frac{1}{X_{Fe}+K_{MO}X_M}(X_{Fe}\Delta g_{FeO}+K_{MO}X_M\Delta g_{MO})-\frac{X_{Fe}X_M}{(X_{Fe}+X_M)^2}\Delta g_{FeM}\right] \tag{50}$$

The derived expressions for γ_M and γ_O represent the explicit forms that show dependence on the composition and temperature of the solution. Thus, γ_M and γ_O can be calculated directly as functions of composition and temperature, which eliminates the need for additional steps such as internal Gibbs energy minimization.

Substitution of these calculated values of γ_M and γ_O into the equilibrium-constant equation (Eq. (10)) determines the deoxidation equilibrium conditions (X_M and X_O). The conversion of these equilibrium compositions into mass percentages ([%M] and [%O]) is a straightforward process.

Determining the deoxidation equilibria for element M requires the parameters Δg_{FeM} and Δg_{MO}, which represent the Gibbs energy differences of the reactions involving Fe–M and M–O species, respectively. Δg_{FeO} is common in all systems containing Fe and O. In addition, the coordination number Z can be set as a constant value for all elements.

The incorporation of these parameters and values into the model equations enables the accurate prediction of the deoxidation equilibria for element M, providing insights into the deoxidation process of liquid steel.

5. Deoxidation equilibrium calculations using the present model

The present model was applied to describe the deoxidation equilibria of liquid steel. Here, all parameters (Δg_{FeM}, Δg_{FeO}, and Δg_{MO}) were optimized through the study, and their values are listed in Table 1. Table 2 lists the equilibrium constants ($K_{M_xO_y}$) for the deoxidation reactions. These equilibrium constants were determined by considering the Gibbs energy of oxidation involving pure elements from databases, such as FactSage FTOxid database [20–21] for oxides based on Barin's compilation [45] and SGTE database [46] for metal elements.

O activity ($a_{\underline{O}(wt\%)}$) is often reported to be relative to the 1wt% standard state ($a_{\underline{O}(wt\%)}$). This activity is related to the activity relative to the Raoultian standard state (a_O) through the following relationship:

$$a_{\underline{O}(wt\%)} = \frac{100 M_O}{\gamma_O^{\ominus} M_{Fe}} a_O \tag{51}$$

5.1. Al deoxidation in liquid Fe: Fe–Al–O system

The deoxidation equilibria of Al in liquid Fe–Al–O alloys have been extensively investigated through experimental studies [4,11,47–54] and thermodynamic analyses [3,7,11,55]. The data obtained from these studies are typically reported in two ways: O content ([%O]) and $a_{\underline{O}(wt\%)}$ in the 1wt% standard state. The [%O] is often determined using methods such as the inert-gas fusion infrared absorption technique [56–57], and $a_{\underline{O}(wt\%)}$ is measured using solid-oxide electrolyte methods [47–48,58]. In the case of [%O], the total [%O] (soluble and insoluble) in the quenched specimen is usually measured and assumed to represent the "soluble" [%O]. Figs. 3 and 4 present the data measured at 1600°C.

Various thermodynamic analyses were conducted on Al deoxidation equilibria, and one of the present authors applied the MQM in pair approximation [11] (Section 3). The figures display the [%O] calculated using the MQM as a thin blue dotted line. Thus far, this approach is considered the most accurate for the estimation of Al deoxidation equilibria among different thermodynamic analyses owing to its accuracy over a wide composition range. Further details on model calculations can be found in the work of Paek *et al.* [11], whereas the related working principles have been discussed elsewhere [18]. For comparison, the results calculated using other approaches, such as the WIPF, along with parameters suggested by JSPS [55] and the associate solution model [3,7,29], were also included.

Figs. 3 and 4 display the results obtained using the present model (blue lines). The present model demonstrated good agreement with the measured [%O] up to a certain aluminum content ([%Al] = ~10 or lg [%Al] = ~1). It also reasonably described the measured $a_{\underline{O}(wt\%)}$ within the range of experimental measurements (Fig. 4). The present model performed as well as the MQM in describing deoxidation equilibria up to [%Al] = ~10, and this range is sufficient to cover the [%Al] of most practical steel products.

Table 1. Model parameters optimized in the present study

$\Delta g_{FeO} = -130000\ \mathrm{J\cdot mol^{-1}}$

M	Δg_{FeM} / (J·mol^{-1})	Δg_{MO} / (J·mol^{-1})	$\lg K_{MO}\left(= -\frac{\Delta g_{MO} - \Delta g_{FeO}}{2RT}\right)$
Al	−50000	−260000	$7818/T$
B	−43000	−225000	$5713/T$
C	−77000	−170000	$2406/T$
Ca	10000	−450000	$19245/T$
Ce	−40000	−350000	$13231/T$
Cr	8000	−200000	$4210/T$
La	−30000	−450000	$19245/T$
Mg	10000	−400000	$16238/T$
Mn	−1000	−180000	$3007/T$
Nb	7000	−240000	$6615/T$
Si	−95000	−190000	$3608/T$
Ti	−40000	−270000	$8420/T$
V	−15000	−240000	$6615/T$
Zr	−60000	−360000	$13832/T$

Table 2. Equilibrium constant of deoxidation reactions used in the present study [20–21,45–46]. $\lg K_{M_xO_y} = -\Delta G^{\ominus}_{M_xO_y}/(2.303RT)$

$2Al(l) + 3O(l) = Al_2O_3(s)$	$\lg K_{Al_2O_3} = 86839.9/T - 11.7$
$2B(l) + 3O(l) = B_2O_3(l)$	$\lg K_{B_2O_3} = 67721.0/T - 7.6$
$C(l) + O(l) = CO(g)$	$\lg K_{CO} = 12007.2/T + 4.8$
$Ca(l) + O(l) = CaO(s)$	$\lg K_{CaO} = 33025.9/T - 4.0$
$2Ce(l) + 3O(l) = Ce_2O_3(s)$	$\lg K_{Ce_2O_3} = 100194.1/T - 14.5$
$Fe(l) + 2Cr(l) + 4O(l) = FeCr_2O_4(s)$	$\lg K_{FeCr_2O_4} = 79025.9/T - 12.4$
$2Cr(l) + 3O(l) = Cr_2O_3(s)$	$\lg K_{Cr_2O_3} = 60410.0/T - 9.0$
$2La(l) + 3O(l) = La_2O_3(s)$	$\lg K_{La_2O_3} = 93488.5/T - 10.0$
$Mg(l) + O(l) = MgO(s)$	$\lg K_{MgO} = 31306.7/T - 4.2$
$Mn(l) + 2Al(l) + 4O(l) = MnAl_2O_4(s)$	$\lg K_{MnAl_2O_4} = 109703/T - 14.8$
$Mn(l) + O(l) = MnO(s)$	$\lg K_{MnO} = 21560.9/T - 3.2$
$2Nb(l) + 5O(l) = Nb_2O_5(s)$	$\lg K_{Nb_2O_5} = 102568.3/T - 15.6$
$Nb(l) + 2O(l) = NbO_2(s)$	$\lg K_{NbO_2} = 41217.3/T - 5.4$
$Si(l) + 2O(l) = SiO_2(s)$	$\lg K_{SiO_2} = 49445.9/T - 7.2$
$2Ti(l) + 3O(l) = Ti_2O_3(s)$	$\lg K_{Ti_2O_3} = 78680.3/T - 8.9$
$3Ti(l) + 5O(l) = Ti_3O_5(s)$	$\lg K_{Ti_3O_5} = 127859.1/T - 14.4$
$Ti(l) + O(l) = TiO(s)$	$\lg K_{TiO} = 28206.2/T - 3.2$
$Fe(l) + 2V(l) + 4O(l) = FeV_2O_4(s)$	$\lg K_{FeV_2O_4} = 82231.3/T - 12.4$
$2V(l) + 3O(l) = V_2O_3(s)$	$\lg K_{V_2O_3} = 62455.8/T - 7.5$
$V(l) + O(l) = VO(s)$	$\lg K_{VO} = 22621.1/T - 2.8$
$Zr(l) + 2O(l) = ZrO_2(s)$	$\lg K_{ZrO_2} = 56890.1/T - 6.3$

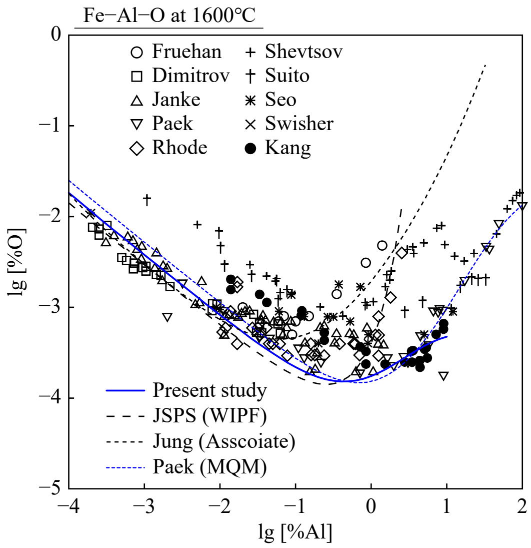

Fig. 3. Deoxidation equilibria of Al in liquid steel at 1600°C: [%O] as a function of [%Al]. Experimental data were obtained from Refs. [4,11,47–54]. Thermodynamic calculations reported in the literature are also shown [7,11,55].

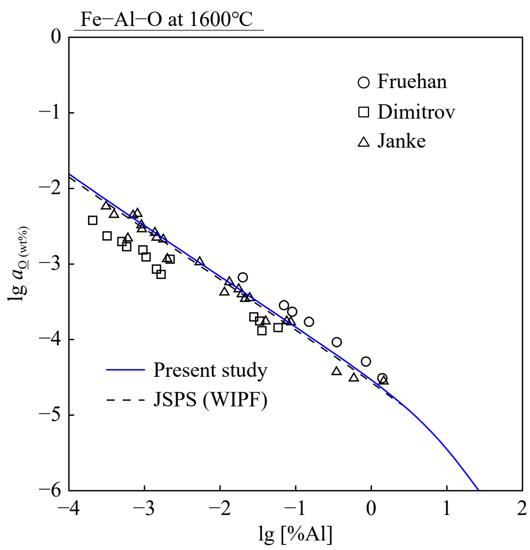

Fig. 4. Deoxidation equilibria of Al in liquid steel at 1600°C: $a_{\underline{O}(wt\%)}$ (with respect to 1wt% standard state) as a function of [%Al]. Experimental data were taken from Refs. [47–49]. Thermodynamic calculation reported in the literature is also shown [55].

To obtain these results at 1600°C, the following model parameters were deduced (kJ·mol^{-1}):

$$\Delta g_{FeO} = -130,\ \Delta g_{FeAl} = -50,\ \Delta g_{AlO} = -260 \tag{52}$$

along with $Z = 2$. The deoxidation equilibria for a given set of model parameters were calculated and compared with experimental data. The procedure was repeated until a satisfactory result was obtained. Then, the optimized model parameters were finally obtained. Furthermore, $K_{Al_2O_3}$ in Eq. (10) was provided as a function of temperature (Table 2). Notably, Δg_{FeO} was optimized to describe not only Al deoxidation but also the deoxidation equilibria of other elements M. This will be shown in subsequent sections.

Although the parameters Δg_{FeO}, Δg_{FeAl}, and Δg_{AlO} were newly optimized in the present study, they showed very similar sizes of excess Gibbs energy for each binary system, which is proportional to the product between the coordination number Z and Δg_{ij} (Eq. (33)).

Fig. 5 displays the calculated Al deoxidation equilibria ([%O] and $a_{\underline{O}(wt\%)}$) over the temperature range of 1550–1850°C, along with available experimental data [11,59–60]. Within the composition range of Al ([%Al] < ~10), the model demonstrated good agreement with experimental data across the entire temperature range.

5.2. Deoxidation of liquid Fe by other elements relevant to steel production: Fe–M–O system (M = Si, Ti, Mn, Cr, and C)

The deoxidation equilibria of other deoxidizing elements (M) in Fe–M–O alloys was described using the present model. Figs. 6–9 illustrate the deoxidation equilibria ([%O] and $a_{\underline{O}(wt\%)}$) of Si, Ti, Mn, and Cr, respectively. Comparison was conducted between experimental data reported in the literature [9,47,49,61–80] and model calculations. Similar to the approach presented in Section 5.1, a coordination number (Z)

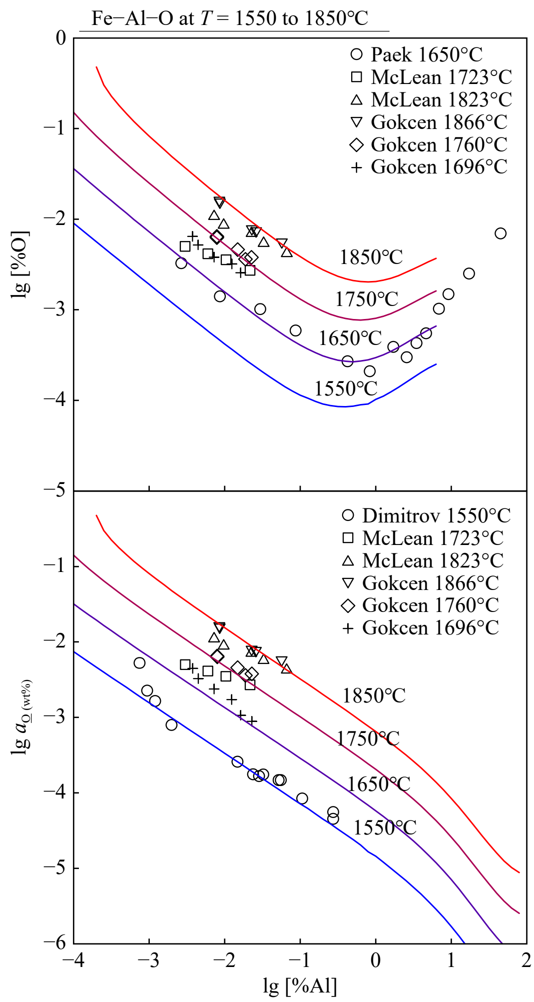

Fig. 5. Deoxidation equilibria of Al in liquid steel at various temperatures: [%O] and $a_{\underline{O}(wt\%)}$ (with respect to 1wt% standard state) as a function of [%Al]. Experimental data were taken from Refs. [11,59–60]. Lines represent the results calculated in the present study.

of 2 was assumed for all elements, and the Δg_{FeO} was maintained at −130 kJ·mol^{-1}. The calculation for each Fe–M–O solution required two additional parameters, namely, Δg_{FeM} and Δg_{MO}, which were set as constants, respectively. The equilibrium constants ($K_{M_xO_y}$) in Eq. (10) were obtained from reliable sources [20–21,46], so these are not the model parameters. As a result, the advantage of the present model in requiring a minimal number of model parameters in calculations has been demonstrated.

In addition to the deoxidation equilibria of deoxidizing elements, the investigation focused on the solubility of O in liquid Fe–C–O alloys. As shown in Fig. 10, the [%O] in liquid Fe–C–O alloys was calculated at various temperatures and P_{CO} = 1 atm and presented along with the reported experimental data [81–87].

5.3. Deoxidation of liquid Fe by strong deoxidizing elements

In the thermodynamic modeling of deoxidation equilibria, the deoxidation of liquid steel by strong deoxidizing elements, such as Ca, presents a challenge. The deoxidation

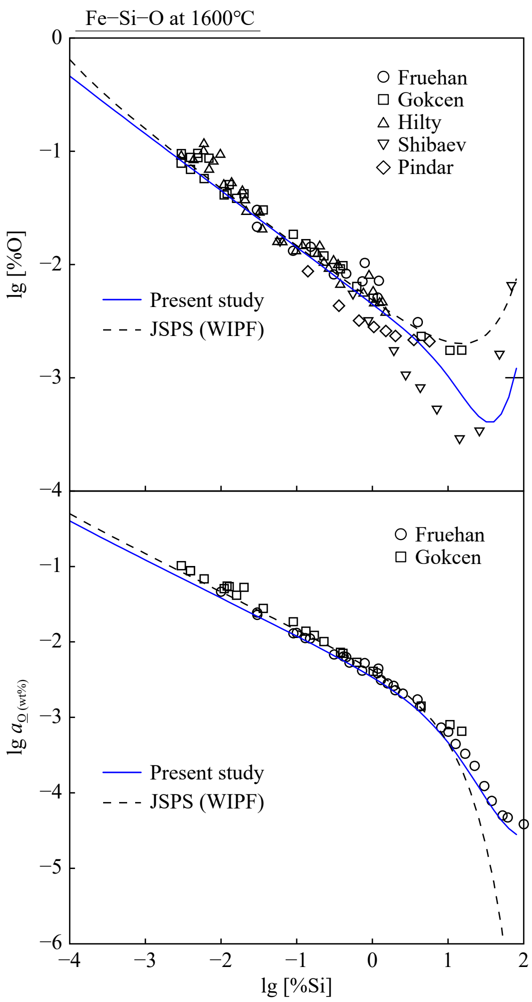

Fig. 6. Deoxidation equilibria of Si in liquid steel at 1600°C: [%O] and $a_{\underline{O}(wt\%)}$ (with respect to 1wt% standard state) as a function of [%Si]. Experimental data were taken from Refs. [61–65]. Thermodynamic calculation reported in the literature is also shown [55].

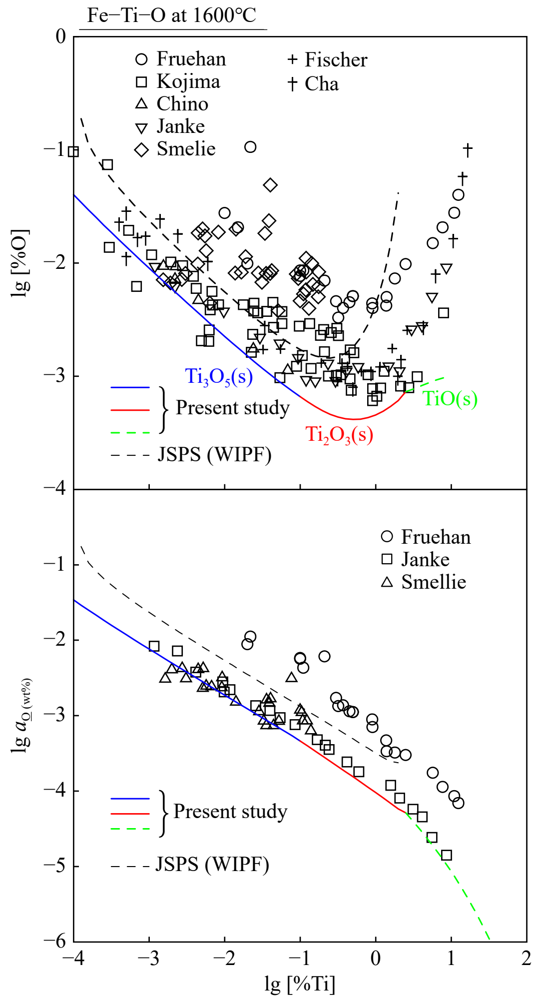

Fig. 7. Deoxidation equilibria of Ti in liquid steel at 1600°C: [%O] and $a_{\underline{O}(wt\%)}$ (with respect to 1wt% standard state) as a function of [%Ti]. Experimental data were obtained from Refs. [9,47,49,66–69]. Thermodynamic calculation reported in the literature is also shown [55].

curve of Ca deoxidation exhibited an unusual shape when the random mixing of atoms was assumed [88]. However, the accuracy of the reported experimental data is also a concern due to limitations in chemical analysis techniques [5,88–90]. The overestimation of [%O] in the experimental data is possible due to analysis limitations [91–93]. Therefore, caution must be exercised in the performance assessment of any model in the absence of reliable experimental data on deoxidation equilibria.

In the present study, the developed model was applied to calculate the deoxidation equilibria of liquid steel by Ca, and the results are shown in Fig. 11, including those at conventional logarithmic scale (upper panel) and normal scale (lower panel) [88,94–98]. The calculated [%O] in the logarithmic scale differs from that in previous figures (Figs. 3 and 5–10). The lower panel in Fig. 11 presents the same results but in a more dilute concentration region in the normal scale. A minimum [%O] was observed, as discussed by one of the present authors [99].

Fig. 12 displays the deoxidation equilibria of liquid steel by cerium (Ce). A lower [%O] was calculated compared with

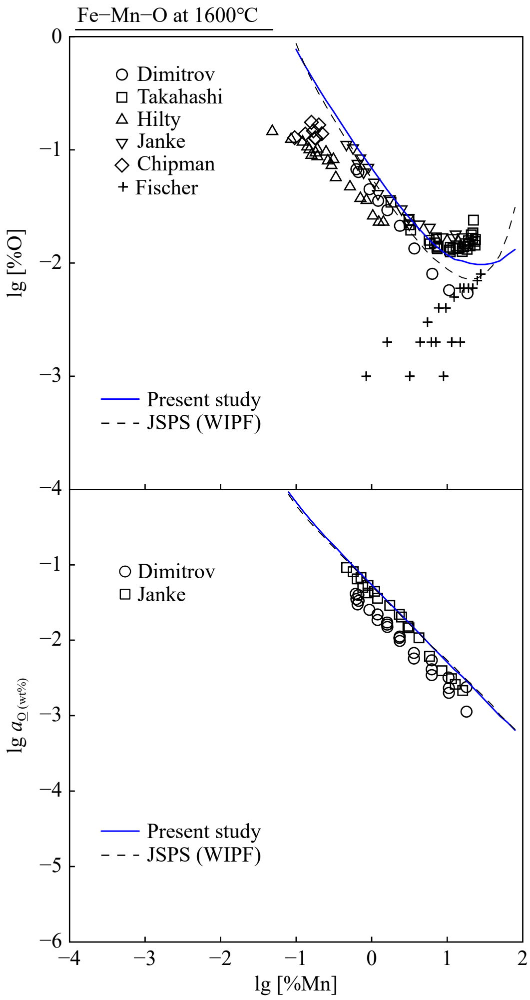

Fig. 8. Deoxidation equilibria of Mn in liquid steel at 1600°C: [%O] and $a_{\underline{O}(wt\%)}$ (with respect to 1wt% standard state) as a function of [%Mn]. Experimental data were taken from Refs. [63,69–73]. Thermodynamic calculation reported in the literature is also shown [55].

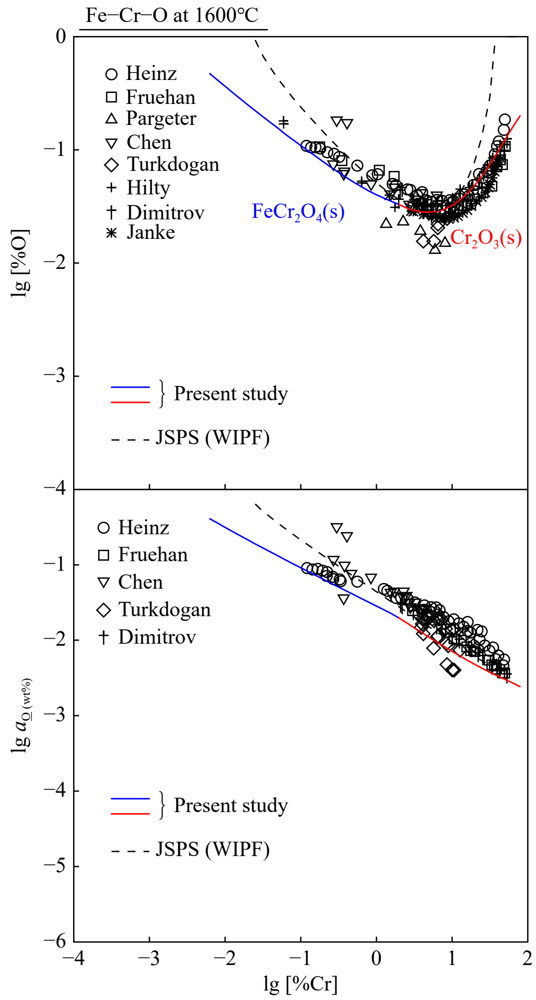

Fig. 9. Deoxidation equilibria of Cr in liquid steel at 1600°C: [%O] and $a_{\underline{O}(wt\%)}$ (with respect to 1wt% standard state) as a function of [%Cr]. Experimental data were taken from Refs. [49,74–80]. Thermodynamic calculation reported in the literature is also shown [55].

the reported experimental data [100–101]. However, the calculated $a_{\underline{O}(wt\%)}$ shows very good agreement with the data from the work of Janke and Fischer [102].

Appendix A in Supplementary Information provides the model calculations for deoxidation equilibria by other strong deoxidizers, such as Mg, La, and Zr.

5.4. Deoxidation of liquid Fe by other elements relevant to steel production: Fe–M–O system (M = Nb, V, and B)

Nb, V, and B are also commonly added to liquid steel as alloying elements. Appendix B in Supplementary Information presents the model calculations for the deoxidation equilibria involving these elements.

6. Discussion

6.1. Application of the present model in complex deoxidation

The present model can be readily extended to multicomponent liquid-steel systems, where multiple deoxidizing metallic elements coexist with Fe and O. Appendix C in Sup-

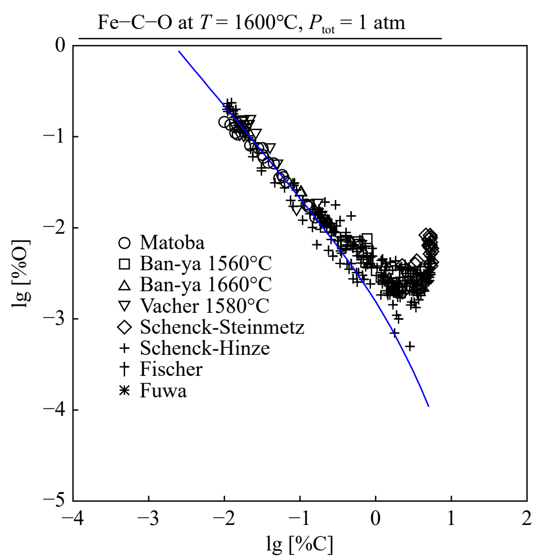

Fig. 10. Deoxidation equilibria of C in liquid steel at 1600°C: [%O] as a function of [%C]. Experimental data were taken from Refs. [81–87].

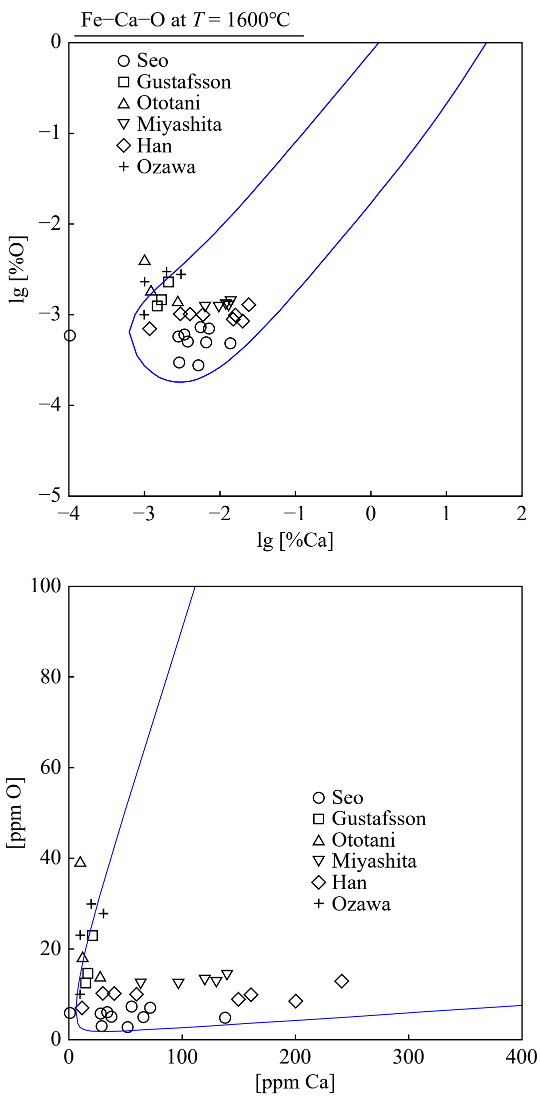

Fig. 11. Deoxidation equilibria of Ca in liquid steel at 1600°C: [%O] as a function of [%Ca]. Experimental data were taken from [88,94–98].

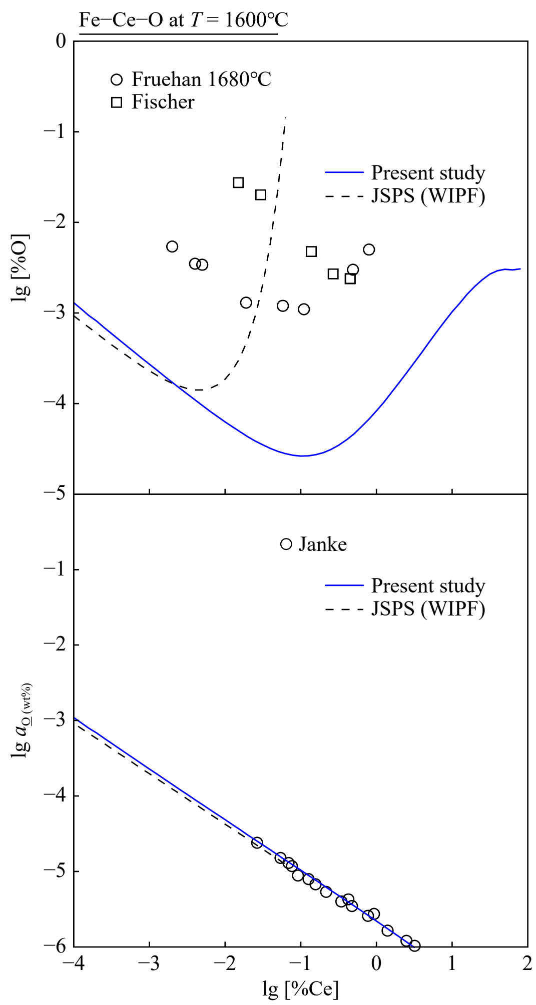

Fig. 12. Deoxidation equilibria of Ce in liquid steel at 1600°C: [%O] and $a_{\underline{O}(wt\%)}$ (with respect to 1wt% standard state) as a function of [%Ce]. Experimental data were collected from [100–101]. Thermodynamic calculation reported in the literature is also shown [55].

plementary Information provides the expressions for the activity coefficients of any metallic element (M) and that of O (Eqs. (C.3) and (C.4)). To demonstrate the applicability of the model to complex deoxidation equilibria, a case study involving high-Mn and high-Al steel was conducted.

Fig. 13 displays the calculated oxide stability diagram of the Fe–Al–Mn–O system; this system represents the equilibrium conditions for oxide formation, along with the reported experimental data [25,70,103–106]. The construction principles observed in the oxide stability diagrams have been discussed by Kang and Jung [107]. The calculated results obtained from the present model agree well with experimental data, highlighting the effectiveness of the model in describing complex deoxidation equilibria in high-Mn–high-Al steel systems. However, contrary to the oxide stability diagram proposed by one of the present authors' previous studies [25], the present calculations disregarded the stable region of liquid oxide. This omission was due to the characteristic calculation logic used in the present study, as pointed out by the present author's other article [107]. Therefore, the present calculation approach can only be used in solid equilibrium-oxide phases with a low nonstoichiometry, such as Al_2O_3, MnO, or $MnAl_2O_4$.

6.2. Coupling to CFD simulation

The present thermodynamic model was utilized to develop a reoxidation simulator for tundish liquid steel during the casting process. The designed simulator calculates the extent of reoxidation, referring to the consumption of the deoxidizing element caused by the presence of a tundish open eye (TOE). The thermodynamic model was incorporated into a user-defined function in the CFD software Ansys Fluent (version 18.2) to determine the deoxidation equilibria of Al-killed ultra-low carbon steel.

Thermodynamics was coupled to fluid dynamics to simulate reoxidation conditions, including the concentrations of soluble Al, soluble O, and suspended alumina inclusions in liquid steel within the tundish at each time and location. A reoxidation simulator of liquid steel in a tundish was developed using the present thermodynamic model to calculate the extent of reoxidation (consumption of deoxidizing element) due to a TOE during the casting process. The thermo-

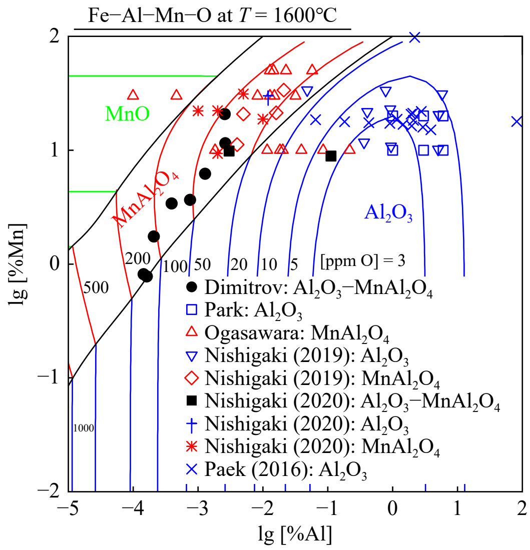

Fig. 13. Oxide stability diagram of Fe–Al–Mn–O system calculated using the present thermodynamic model. Experimental data were obtained from [25,70,103–106].

dynamic model was programmed into a CFD user-defined function of Ansys Fluent (version 18.2) [108] to determine the deoxidation equilibria of Al-killed ultra-low C steel. Non-steady–state fluid dynamic calculations were performed using the CFD code. The direct coupling of thermodynamics to fluid dynamics enabled the simulation of the extent of reoxidation (concentrations of soluble Al, soluble O, and suspended alumina inclusion in liquid steel in the tundish) at each time and location. The reoxidation conditions of the liquid steel are as follows: (1) The liquid steel consisted of Fe–Al–O and represented ultra-low carbon steel with initial compositions of [%Al] = 0.052 and [%O] = 0.0003. The steel initially filled the tundish and was covered by a tundish flux, which was assumed to be a nonreactive liquid phase with a thickness of 20 mm. (2) Liquid steel of the same initial composition flowed into the tundish through the shroud nozzle, creating a TOE. The air entered through the TOE and oxidized the liquid steel via reaction (3). (3) The flow rates of the incoming steel through the shroud nozzle and the outgoing steel through the submerged-entry nozzle were balanced, resulting in a constant liquid-steel depth in the tundish.

Fig. 14 presents an example of the simulator calculation, specifically 200 s after the casting process was initiated. The depicted tundish represents a quarter section of an actual operational tundish in a casting shop at a 1:1 scale. The simulation yielded spatial distributions of the mass fractions of soluble aluminum, soluble oxygen content, and alumina content in the liquid steel. The TOE was observed near the liquid-steel surface between the shroud nozzle and the weir. The mass fraction of soluble Al noticeably decreased, and the [%Al] increased near the TOE.

The simulation was performed through the direct coupling of the CFD code to the thermodynamic model for deoxidation within the CFD framework. Further details on simulator development will be published separately.

6.3. Applicable range of the present model and its limit

The MQM in the pair approximation has been successfully applied in the accurate description of deoxidation equilibria across a wide range of compositions and temperatures

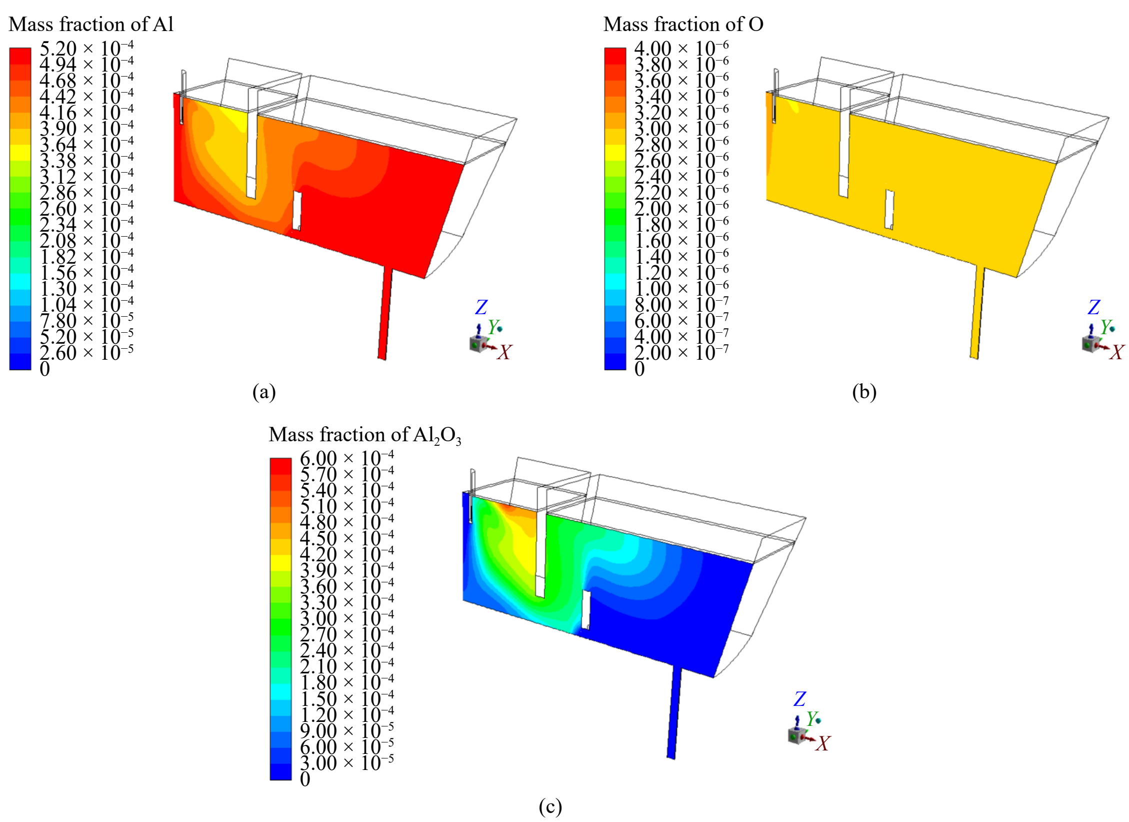

Fig. 14. Snapshots of liquid steel in the tundish (a quarter of 1:1 scale tundish) simulated by the CFD coupled with the present deoxidation model: (a) Al (soluble) content, (b) O (soluble) content, and (c) Al_2O_3 (inclusion) content.

[11,25].

In the present study, a new model approach based on the MQM was developed to provide a simpler but still accurate method of calculating deoxidation equilibria. The present model was successfully applied overall, and unsatisfactory results were obtained in a few cases, particularly at high concentrations of deoxidizing elements (Figs. 3, 5, and 7). The assumption on a constant pair formation energy (Δg_{FeM} in Eq. (16)) may be responsible for these discrepancies. Previous thermodynamic modeling research on Fe–M binary systems using MQM often considered Δg_{FeM} to be composition dependent, either through composition variables or pair fraction variables. In the present study, the complexity associated with composition-dependent Δg_{FeM} was intentionally avoided for simplicity. However, expressing Δg_{FeM} as a function of composition will lead to intricate expressions for the activity coefficients of M and O (Eqs. (49), (50), (C.3), and (C.4)), which were not pursued in the present study.

6.4. Accuracy of the measured [%O]

Challenges have been observed in the thermodynamic modeling of deoxidation equilibria of liquid steel by strong deoxidizing elements, such as Ca, Mg, Zr, La, and Ce, not only in the present study but also in previous literature [88,90]. Figs. 12 (Ce), A.2 (La), and A.3 (Zr) exhibit good agreement between the model calculations and experimental data for $a_{\underline{\mathrm{O}}(\mathrm{wt\%})}$), indicating a successful prediction of $a_{\underline{\mathrm{O}}(\mathrm{wt\%})}$. However, a discrepancy was observed in the [%O] values between the model calculations and experimental data. This discrepancy has been discussed by several researchers [88–90]. Hillert and Selleby [89] pointed out potential systematic errors in the measured solubilities of Ca-deoxidized liquid steel. Huang [90] also expressed skepticism regarding the accuracy of the measured [%O] in Zr-deoxidized steel. Gustafsson and Malmberg [88] cautioned about the interpretation of the currently used experimental techniques.

The measurement of [%O] in steel specimens through the gas-fusion infrared absorption method [56–57,91] is typically intended to determine the total [%O], including soluble and insoluble O. The overestimation of the soluble [%O] is possible due to the presence of oxide inclusions (insoluble O). Recent advancements in analysis methods allow for the simultaneous measurement of soluble and insoluble [%O], which can help in the refined determination of [%O] in steel specimens [91–93].

7. Conclusions

In the present study, thermodynamic modeling of deoxidation equilibria of liquid steel considered the strong interaction between metal and O, avoiding the assumption of simple random mixing. The model is a limiting case of the quasi-chemical model, with the assumption of constant coordination numbers, constant pair-exchange energies, complete SRO between metal and O, and random mixing of metallic components. The equilibrium constant equation was solved to determine the deoxidation equilibria. The activity coefficients of M and O were expressed as explicit functions of composition and temperature, accounting for nonrandom mixing between metal and O. Importantly, the present model skips the minimization of complex internal Gibbs energy, resulting in a computationally efficient approach for the high-accuracy calculation of deoxidation equilibria of liquid steel.

The present model can be easily coupled with other simulation codes, such as CFD, for fluid flow simulations that involve deoxidation phenomena. This coupling considerably reduces the computation time by directly incorporating the deoxidation equilibria calculation into the simulation code.

Conflict of Interest

Youn-Bae Kang is an editorial board member for this journal and was not involved in the editorial review or the decision to publish this article. The authors claim no conflicts of interest.

Supplementary Information

The online version contains supplementary material available at https://doi.org/10.1007/s12613-023-2766-7.

References

[1] L.F. Zhang and B.G. Thomas, State of the art in evaluation and control of steel cleanliness, *ISIJ Int.*, 43(2003), No. 3, p. 271.

[2] Y. Sahai and T. Emi, *Tundish Technology for Clean Steel Production*, World Scientific, Singapore, 2007.

[3] K. Wasai and K. Mukai, Thermodynamic analysis of Fe−Al−O liquid alloy equilibrated with α-Al_2O_3(s) by an associated solution model, *J. Jpn. Inst. Met. Mater.*, 52(1988), No. 11, p. 1088.

[4] H. Suito, H. Inoue, and R. Inoue, Aluminium−oxygen equilibrium between CaO−Al_2O_3 melts and liquid iron, *ISIJ Int.*, 31(1991), No. 12, p. 1381.

[5] T. Kimura and H. Suito, Calcium deoxidation equilibrium in liquid iron, *Metall. Mater. Trans. B*, 25(1994), No. 1, p. 33.

[6] H. Itoh, M. Hino, and S. Ban-Ya, Assessment of Al deoxidation equilibrium in liquid iron, *Tetsu-to-Hagané*, 83(1997), No. 12, p. 773.

[7] I.H. Jung, S.A. Decterov, and A.D. Pelton, A thermodynamic model for deoxidation equilibria in steel, *Metall. Mater. Trans. B*, 35(2004), No. 3, p. 493.

[8] T. Miki and M. Hino, Numerical analysis on Si deoxidation of molten Fe−Ni and Ni−Co alloys by quadratic formalism, *ISIJ Int.*, 44(2004), No. 11, p. 1800.

[9] W.Y. Cha, T. Nagasaka, T. Miki, Y. Sasaki, and M. Hino, Equilibrium between titanium and oxygen in liquid Fe−Ti alloy coexisted with titanium oxides at 1873 K, *ISIJ Int.*, 46(2006), No. 7, p. 996.

[10] A. Hayashi, T. Uenishi, H. Kandori, T. Miki, and M. Hino, Aluminum deoxidation equilibrium of molten Fe–Ni alloy coexisting with alumina or hercynite, *ISIJ Int.*, 48(2008), No. 11, p. 1533.

[11] M.K. Paek, J.J. Pak, and Y.B. Kang, Aluminum deoxidation equilibria in liquid iron: Part II. thermodynamic modeling, *Metall. Mater. Trans. B*, 46(2015), No. 5, p. 2224.

[12] C. Wagner, *Thermodynamics of Alloys*, Addison-Wesley Pub.

Co., Reading, MA, 1951, p. 51.
[13] C.H.P. Lupis and J. F. Elliott, The relationship between the interaction coefficients epsilon and e, *Trans. Metall. Soc. AIME*, 233(1965), p. 257.
[14] C.H.P. Lupis, *Chemical Thermodynamics of Materials*, Simon & Schuster (Asia) Pte Ltd., Singapore, 1993.
[15] L.S. Darken, Thermodynamics of binary metallic solutions, *Trans. Metall. Soc. AIME*, 239(1967), p. 80.
[16] R. Schuhmann, Solute interactions in multicomponent solutions, *Metall. Trans. B*, 16(1985), No. 4, p. 807.
[17] A.D. Pelton, The polynomial representation of thermodynamic properties in dilute solutions, *Metall. Mater. Trans. B*, 28(1997), No. 5, p. 869.
[18] Y.B. Kang, Thermodynamic modeling of liquid steel, *ISIJ Int.*, 60(2020), No. 12, p. 2717.
[19] Y.B. Kang, The uniqueness of a correction to interaction parameter formalism in a thermodynamically consistent manner, *Metall. Mater. Trans. B*, 51(2020), No. 2, p. 795.
[20] C.W. Bale, E. Bélisle, P. Chartrand, *et al*., FactSage thermochemical software and databases—Recent developments, *Calphad*, 33(2009), No. 2, p. 295.
[21] C.W. Bale, E. Bélisle, P. Chartrand, *et al*., FactSage thermochemical software and databases, 2010–2016, *Calphad*, 54(2016), p. 35.
[22] J.O. Andersson, T. Helander, L. Höglund, P.F. Shi, and B. Sundman, Thermo-Calc & DICTRA, computational tools for materials science, *Calphad*, 26(2002), No. 2, p. 273.
[23] S. Petersen and K. Hack, The thermochemistry library ChemApp and its applications, *Int. J. Mater. Res.*, 98(2007), No. 10, p. 935.
[24] Y. Cho, H. Cho, S. Han, *et al*., A chemical reaction-fluid dynamics coupled model for Al reoxidation in tundish by open eye formation, [in] *8th International Congress on the Science and Technology of Steelmaking*, Warredale, PA, 2022, p. 167.
[25] M.K. Paek, K.H. Do, Y.B. Kang, I.H. Jung, and J.J. Pak, Aluminum deoxidation equilibria in liquid iron: Part III—Experiments and thermodynamic modeling of the Fe–Mn–Al–O system, *Metall. Mater. Trans. B*, 47(2016), No. 5, p. 2837.
[26] G.K. Sigworth and J.F. Elliott, The thermodynamics of liquid dilute iron alloys, *Met. Sci.*, 8(1974), No. 1, p. 298.
[27] L. S. Darken, Thermodynamics of ternary metallic solutions, *Trans. Metall. Soc. AIME*, 239(1967), p. 90.
[28] C.W. Bale and A.D. Pelton, The unified interaction parameter formalism: Thermodynamic consistency and applications, *Metall. Trans. A*, 21(1990), No. 7, p. 1997.
[29] D. Bouchard and C.W. Bale, Thermochemical properties of iron-rich liquid solutions containing oxygen and aluminum, *J. Phase Equilib.*, 16(1995), No. 1, p. 16.
[30] A.D. Pelton, S.A. Degterov, G. Eriksson, C. Robelin, and Y. Dessureault, The modified quasichemical model I—Binary solutions, *Metall. Mater. Trans. B*, 31(2000), No. 4, p. 651.
[31] A.D. Pelton, P. Chartrand, and G. Eriksson, The modified quasi-chemical model: Part IV. Two-sublattice quadruplet approximation, *Metall. Mater. Trans. A*, 32(2001), No. 6, p. 1409.
[32] J. Lehmann and L. Zhang, The generalized central atom for metallurgical slags and high alloyed steel grades, *Steel Res. Int.*, 81(2010), No. 10, p. 875.
[33] E.A. Guggenheim, Statistical thermodynamics of mixtures with non-zero energies of mixing, *Proc. R. Soc. Lond. A*, 183(1944), No. 993, p. 213.
[34] Y.B. Kang, Pelton A.D., P. Chartrand, and C.D Fuerst, Critical evaluation and thermodynamic optimization of the Al–Ce, Al–Y, Al–Sc and Mg–Sc binary systems, *Calphad*, 32(2008), No. 2, p. 413.
[35] Y.B. Kang and Pelton A.D, Modeling short-range ordering in liquids: The Mg–Al–Sn system, *Calphad*, 34(2010), No. 2, p. 180.
[36] Y.B. Kang and A.D. Pelton, The shape of liquid miscibility gaps and short-range-order, *J. Chem. Thermodyn.*, 60(2013), p. 19.
[37] Y.B. Kang, I.H. Jung, S.A. Decterov, A.D. Pelton, and H.G. Lee, Critical thermodynamic evaluation and optimization of the CaO−MnO−SiO_2 and CaO−MnO−Al_2O_3 systems, *ISIJ Int.*, 44(2004), No. 6, p. 965.
[38] Y.B. Kang, I.H. Jung, and H.G. Lee, Critical thermodynamic evaluation and optimization of the MnO–"TiO_2" –"Ti_2O_3" system, *Calphad*, 30(2006), No. 3, p. 235.
[39] Y.B. Kang, I.H. Jung, and H.G. Lee, Critical thermodynamic evaluation and optimization of the MnO–SiO_2–"TiO_2" –"Ti_2O_3" system, *Calphad*, 30(2006), No. 3, p. 226.
[40] Y.B. Kang and J.H. Lee, Reassessment of oxide stability diagram in the Fe–Al–Ti–O system, *ISIJ Int.*, 57(2017), No. 9, p. 1665.
[41] Y.B. Kang and A.D. Pelton, Thermodynamic model and database for sulfides dissolved in molten oxide slags, *Metall. Mater. Trans. B*, 40(2009), No. 6, p. 979.
[42] R. Piao, D.H. Woo, H.G. Lee, and Y.B. Kang, A thermodynamic model and database for oxysulfide inclusions containing Ca−Mn−Si−Al−O−S and its application to prediction of inclusions evolution in steels, *AIST Trans.*, 11(2014), No. 5, p. 218.
[43] D.G. Kim, M.A. Van Ende, C. van Hoek, C. Liebske, S. van der Laan, and I.H. Jung, A critical evaluation and thermodynamic optimization of the CaO−CaF_2 system, *Metall. Mater. Trans. B*, 43(2012), No. 6, p. 1315.
[44] C.B. Alcock and F.D. Richardson, Dilute solutions in alloys, *Acta Metall.*, 8(1960), No. 12, p. 882.
[45] I. Barin, O. Knacke, and O. Kubaschewski, *Thermochemical Properties of Inorganic Substances*, Springer Berlin Heidelberg, Berlin, Heidelberg, 1977.
[46] A.T. Dinsdale, SGTE data for pure elements, *Calphad*, 15(1991), No. 4, p. 317.
[47] R.J. Fruehan, Activities in liquid Fe–Al–O and Fe–Ti–O alloys, *Metall. Trans.*, 1(1970), No. 12, p. 3403.
[48] S. Dimitrov, A. Weyl, and D. Janke, Control of the aluminium-oxygen reaction in pure iron melts, *Steel Res.*, 66(1995), No. 1, p. 3.
[49] D. Janke and W.A. Fischer, Desoxidationsgleichgewichte von titan, aluminium und zirconium in eisenschmelzen Bei 1600°C, *Archiv für das Eisenhüttenwesen*, 47(1976), No. 4, p. 195.
[50] L.E. Rohde, A. Choudhury, and M. Wahlster, Neuere untersuchungen über das aluminium-sauerstoff-gleichgewicht in eisenschmelzen, *Archiv für das Eisenhüttenwesen*, 42(1971), No. 3, p. 165.
[51] V. Shevtsov, Thermodynamics of oxygen solutions in the Fe–Al system, *Russ. Metall.*, (1981), No. 1, p. 52.
[52] J.D. Seo, S.H. Kim, and K.R. Lee, Thermodynamic assessment of the Al deoxidation reaction in liquid iron, *Steel Res.*, 69(1998), No. 2, p. 49.
[53] J. Swisher, Note on the aluminum-oxygen interaction in liquid iron, *AIME Met. Soc. Trans.*, 239(1967), No. 1, p. 123.
[54] Y. Kang, M. Thunman, S.C. Du, T. Morohoshi, K. Mizukami, and K. Morita, Aluminum deoxidation equilibrium of molten iron–aluminum alloy with wide aluminum composition range at 1 873 K, *ISIJ Int.*, 49(2009), No. 10, p. 1483.
[55] Japan Society for the Promotion of Science, *Steelmaking Data Sourcebook*, Gordon & Breach Science, New York, 1988.
[56] R. Inoue and H. Suito, Determination of oxygen in iron-alu-

minum alloy by inert gas fusion-infrared absorptiometry, *Mater. Trans. JIM*, 32(1991), No. 12, p. 1164.

[57] LECO Corporation, *ON836 Oxygen/Nitrogen Analyzer Instruction Manual*, St. Joseph, MI, 2013.

[58] R. Fruehan, L. Martonik, and E. Turkdogan, Development of a galvanic cell for the determination of oxygen in liquid steel, *Trans. Met. Soc. AIME*, 245(1969), No. 7, p. 1501.

[59] A. McLean and H. Bell, Experimental study of the reaction Al_2O_3 + $3H_2$ = $3H_2O$ + 2Al, *J. Iron Steel Inst.*, 203(1965), p. 123.

[60] N.A. Gokcen and J. Chipman, Aluminum-oxygen equilibrium in liquid iron, *JOM*, 5(1953), No. 2, p. 173.

[61] R.J. Fruehan, The thermodynamic properties of liquid Fe–Si alloys, *Metall. Trans.*, 1(1970), No. 4, p. 865.

[62] N.A. Gokcen and J. Chipman, Silicon-oxygen equilibrium in liquid iron, *JOM*, 4(1952), No. 2, p. 171.

[63] D.C. Hilty and W. Crafts, Solubility of oxygen in liquid iron containing silicon and manganese, *JOM*, 2(1950), No. 2, p. 425.

[64] S.S. Shibaev, P.V. Krasovskii, and K.V. Grigorovitch, Solubility of oxygen in iron–silicon melts in equilibrium with silica at 1873 K, *ISIJ Int.*, 45(2005), No. 9, p. 1243.

[65] S. Pindar and M.M. Pande, Assessment of Si–O equilibria and nonmetallic inclusion characteristics in high silicon steels, *Steel Res. Int.*, 94(2023), art. No.2300115.

[66] Y. Kojima, M. Inouye, and J.I. Ohi, Titanoxyd im gleichgewicht mit eisen-titan-legierungen Bei 1600°C, *Archiv für das Eisenhüttenwesen*, 40(1969), No. 9, p. 667.

[67] H. Chino, Y. Nakamura, E. Tsunetomi, and K. Segawa, The deoxidation with titanium in liquid iron, *Tetsu-to-Hagané*, 52(1966), No. 6, p. 959.

[68] A.M. Smellie and H.B. Bell, Titanium deoxidation reactions in liquid iron, *Can. Metall. Q.*, 11(1972), No. 2, p. 351.

[69] W.A. Fischer and D. Janke, Die aktivität des sauerstoffs in reinen und mangan-, titan-oder borhaltigen eisenschmelzen, *Archiv für das Eisenhüttenwesen*, 42(1971), No. 10, p. 691.

[70] S. Dimitrov, A. Weyl, and D. Janke, Control of the manganese–oxygen reaction in pure iron melts, *Steel Res.*, 66(1995), No. 3, p. 87.

[71] K. Takahashi and M. Hino, Equilibrium between dissolved Mn and O in molten high-manganese steel, *High Temp. Mater. Process.*, 19(2000), No. 1, p. 1.

[72] D. Janke and W. Fischer, Equilibria of chromium and manganese with oxygen in iron melts at 1600°C, *Archiv für das Eisenhüttenwesen*, 47(1976), No. 3, p. 147.

[73] J. Chipman, J.B. Gero, and T.B. Winkler, The manganese equilibrium under simple oxide slags, *JOM*, 2(1950), No. 2, p. 341.

[74] M. Heinz, K. Koch, and D. Janke, Oxygen activities in Cr-containing Fe and Ni-based melts, *Steel Res.*, 60(1989), No. 6, p. 246.

[75] R. Fruehan, Activities in liquid Fe–Cr–O system, *Met. Soc. AIME-Trans*, 245(1969), No. 6, p. 1215.

[76] J.K. Pargeter, The effect of additions of manganese, vanadium and chromium on the activity of oxygen in molten iron, *Can. Metall. Q.*, 6(1967), No. 1, p. 21.

[77] H. Chen and J. Chipman, The chromium–oxygen equilibirum in liquid iron, *Metall. Trans. ASM*, 38(1947), p. 70.

[78] E. Turkdogan, Chromium-oxygen equilibrium in liquid iron, *J. Iron Steel Inst.*, 178(1954), No. 3, p. 278.

[79] D.C. Hilty, W.D. Forgeng, and R.L. Folkman, Oxygen solubility and oxide phases in the Fe–Cr–O system, *JOM*, 7(1955), No. 2, p. 253.

[80] S. Dimitrov, H. Wenz, K. Koch, and D. Janke, Control of the chromium–oxygen reaction in pure iron melts, *Steel Res.*, 66(1995), No. 2, p. 39.

[81] S. Matoba, Equilibrium of carbon and oxygen in molten iron, *Tetsu-to-Hagané*, 20(1934), No. 12, p. 837.

[82] S. Banya and S. Matoba, Activity of carbon and oxygen in liquid iron, *Tetsu-to-Hagané Overseas*, 3(1963), No. 1, p. 21.

[83] H. Schenck, E. Steinmetz, and M. Gloz, Der sauerstoffgehalt in kohlenstoffreichem und kohlenstoffgesättigtem flüssigem eisen Bei 1600°C, *Archiv für das Eisenhüttenwesen*, 39(1968), No. 1, p. 69.

[84] W.A. Fischer and D. Janke, Elektrochemische aufzeichnung des entkohlungsablaufs von eisenschmelzen, *Archiv für das Eisenhüttenwesen*, 42(1971), No. 4, p. 249.

[85] H. Schenck and H. Hinze, Equilibriums of the iron-carbon-oxygen system in the temperature and concentration range of molten steel and the effect of phosphorus, manganese, and sulfur, *Archiv für das Eisenhüttenwesen*, 37(1966), No. 1, p. 545.

[86] T. Fuwa and J. Chipman, Activity of carbon in liquid-iron alloys, *Trans. Metall. Soc. AIME*, 215(1959), p. 708.

[87] T. Fuwa and J. Chipman, The carbon–oxygen equilibria in liquid iron, *Trans. AIME*, 218(1960), p. 887.

[88] S. Gustafsson and P.O. Mellberg, On the free energy interaction between some strong deoxidizers, especially calcium and oxygen in liquid iron, *Scand. J. Metall.*, 9(1980), p. 111.

[89] M. Hillert and M. Selleby, Solubility of CaO and Al_2O_3 in liquid Fe, *Scand. J. Metall.*, 19(1990), p. 23.

[90] W.M. Huang, Oxygen solubility in Fe–Zr–O liquid, *Calphad*, 28(2004), No. 2, p. 153.

[91] H.M. Hong and Y.B. Kang, Simultaneous analysis of soluble and insoluble oxygen contents in steel specimens using inert gas fusion infrared absorptiometry, *ISIJ Int.*, 61(2021), No. 9, p. 2464.

[92] Y.B. Kang, Y.M. Cho, and H.M. Hong, Thermodynamic basis of isothermal carbothermic reduction of oxide in liquid steel for simultaneous analysis of soluble/insoluble oxygen contents in the steel specimens, *Metall. Mater. Trans. B*, 53(2022), No. 4, p. 1980.

[93] Y.M. Cho, D.J. Lee, H.J. Cho, W.Y. Kim, S.W. Han, and Y.B. Kang, Simultaneous analysis of soluble and insoluble oxygen contents in Al-killed steels of various C contents and supersaturation phenomena in the steel, *ISIJ Int.*, 62(2022), No. 8, p. 1705.

[94] J. Seo and S. Kim, Thermodynamic assessment of Al, Mg, and Ca deoxidation reaction for the control of alumina inclusion in liquid steel, *Bull. Korean Inst. Metall. Mater.* (*Korea*), 12(1999), No. 3, p. 402.

[95] T. Ototani, Y. Kataura, and T. Degawa, Deoxidation of liquid iron and its alloys by calcium contained in lime crucible, *Trans. Iron Steel Inst. Jpn.*, 16(1976), No. 5, p. 275.

[96] Y. Miyashita and K. Nishikawa, The deoxidation of liquid iron with calcium, *Tetsu-to-Hagané*, 57(1971), No. 13, p. 1969.

[97] Q.Y. Han, X.D. Zhang, D. Chen, and P.F. Wang, The calcium-phosphorus and the simultaneous calcium–oxygen and calcium–sulfur equilibria in liquid iron, *Metall. Trans. B*, 19(1988), No. 4, p. 617.

[98] M. Ozawa, *The Japan Society for the Promotion of Science, 19th Committee Paper No. 9837*, Iron Steel Institute of Japan, Toyko, 1975, p. 6.

[99] Y.B. Kang, Oxide solubility minimum in liquid Fe–M–O alloy, *Metall. Mater. Trans. B*, 50(2019), No. 6, p. 2942.

[100] R.J. Fruehan, The effect of zirconium, cerium, and lanthanum on the solubility of oxygen in liquid iron, *Metall. Trans.*, 5(1974), No. 2, p. 345.

[101] W.A. Fischer and H. Bertram, Die desoxydation, entschwefelung und entstickung sauerstoff-, schwefel- oder stickstoffhaltiger eisenschmelzen durch die seltenen erdmetalle cer und

lanthan, *Archiv für das Eisenhüttenwesen*, 44(1973), No. 2, p. 87.

[102] D. Janke and W.A. Fischer, Deoxidation equilibria of cerium, lanthanum, and hafnium in liquid iron, *Archiv für das Eisenhüttenwesen*, 49(1978), No. 9, p. 425.

[103] J.H. Park, D.J. Kim, and D.J. Min, Characterization of non-metallic inclusions in high-manganese and aluminum-alloyed austenitic steels, *Metall. Mater. Trans. A*, 43(2012), No. 7, p. 2316.

[104] Y. Ogasawara, T. Miki, and T. Nagasaka, Equilibrium of Al deoxidation in liquid Fe–Mn alloy, *CAMP-ISIJ*, 25(2012), p. 240.

[105] R. Nishigaki and H. Matsuura, Al deoxidation equilibrium of Fe–10–30 mass%Mn melt at 1873 K, *Tetsu-to-Hagané*, 105(2019), No. 3, p. 369.

[106] R. Nishigaki and H. Matsuura, Deoxidation equilibria of Fe–Mn–Al melt with Al_2O_3 or $MnAl_2O_4$ at 1873 and 1773 K, *ISIJ Int.*, 60(2020), No. 12, p. 2787.

[107] Y.B. Kang and S.H. Jung, Oxide stability diagram of liquid steels – Construction and utilization, *ISIJ Int.*, 58(2018), No. 8, p. 1371.

[108] ANSYS, Inc., *Ansys Fluent 12.0*, *Theory Guide*, 2009, p. 67.